Stochastic backscatter of turbulence energy and scalar variance by random subgrid-scale fluxes

By Ulrich Schumann

Deutsche Forschungsanstalt für Luft- und Raumfahrt (DLR), Institut für Physik der Atmosphäre, Oberpfaffenhofen, 82230 Wessling, Germany

For large-eddy simulation with a finite-difference scheme, a simple stochastic subgrid-scale (SGS) model is introduced which describes the effects of random SGS motions on the resolved (filtered) scales of incompressible turbulent motions. The model extends the Smagorinsky–Lilly model by adding realizable random stresses and fluxes which are constructed as quadratic expressions of Gaussian random velocity and temperature fields. The random components reduce the correlations between stresses and strain rates to in between 0.16 and 0.5, in agreement with observations. The random stresses (fluxes) also induce random accelerations (temperature changes) with a k^4 power spectrum. Such random sources backscatter energy (variance) from SGS motions to resolved scale motions when temporally correlated with finite timescales. The timescales are different for momentum and heat flux. The analysis of the model provides an upper estimate of the magnitude of backscatter which is close to previous predictions. The analysis identifies the influence of the quasi-normal assumption and of numerical filters and determines the variance of the pressure fluctuations induced by the random accelerations at grid scales. Backscatter increases the SGS turbulent Prandtl number to a degree depending strongly on the numerical filter. Tests of the model in large-eddy simulation of isotropic turbulence show energy decay rates in close agreement with expected rates when the stochastic SGS model is included. Backscatter cannot be simulated with reduced diffusivities or filter widths.

1. Introduction

The modern study of turbulence was initiated by Osborne Reynolds (1842–1912). The Reynolds number, the Reynolds stresses and the Reynolds analogy between momentum and heat transfer are among the many concepts which still influence our thinking. On the occasion of the centenary of the publication of his paper Reynolds (1895) this contribution intends to demonstrate, in some small way, his influence in the present discussion on the nature of Reynolds stresses in large-eddy simulation models.

Reynolds (1895) started from molecular disorder and introduced various mean values. 'Mean motions' resulting from averaging over small spatial domains eliminate the molecular disorder and result in fluctuating motions that satisfy the Navier–Stokes equations. The steady motion obtained by further averaging was called 'mean-mean-motion' by Reynolds. The fluctuating motions act on the mean-mean-motions in terms of what we call Reynolds stresses. Reynolds (1895) also derived the budget for the turbulent kinetic energy of fluctuating turbulent motions with shear production

Proc. R. Soc. Lond. A (1995) **451**, 293–318
Printed in Great Britain

TEX Paper

and viscous dissipation rates, and many models have been deduced from this budget (Launder *et al.* 1975).

A variant of Reynolds's averaging is used in large-eddy simulation (LES). As proposed by Smagorinsky (1963), Lilly (1967), and Deardorff (1970), a LES distinguishes between fluctuating motions at small scales, below a certain scale Δ, and large-scale or 'large-eddy' motions averaged over regions of that size. Alternatively, one considers the large-eddy motions as those remaining after smoothing the smaller-scale fluctuations with a filter of bandwidth Δ (Leonard 1974). The large-eddy motion field may be resolved by a numerical scheme. When a finite-difference approximation is used for that purpose, then the separating scale is related to the grid scale of the numerical approximation. In this case it is appropriate to talk about subgrid-scale and grid-scale motions. The grid-scale motions satisfy time- and space-dependent equations with subgrid-scale stresses that are formally similar to the classical Reynolds stresses, but are functions of the local flow state and vanish in the limit of zero filter scale. As the classical Reynolds stresses, also the SGS stresses require a model which relates them to the fields at the larger scales for closure. However, the LES model can be more universal than their counterparts for Reynolds stresses because modelling is required only at length-scales Δ, which are smaller than the flow integral scale.

Although LES models capture some of the chaotic nature of real turbulence in that small-amplitude disturbances in the initial or boundary conditions at resolved scales result into possibly large changes of the resultant flow fields, the models are essentially deterministic. Hence, they miss the stochastic effect of random fluctuations at subgrid scales (Fox & Lilly 1972; Rose 1977). The fluctuations at subgrid scales are also solutions of the Navier–Stokes equations and are not strictly random, therefore. But the large number of degrees of freedom and the unknown history of subgrid motions make them appear to be random. This paper deals with random fluctuations of stresses and scalar fluxes. For a general description of stochastic methods see Gardiner (1983). After a review of previous studies on stochastic SGS effects and models in § 2, a new random SGS model is introduced in § 3. Section 4 discusses its effects and § 5 gives the conclusions.

2. On stochastic subgrid-scale models

Most SGS models relate the stresses to the large-scale velocity deformation with some eddy viscosity. The eddy viscosity is the product of a length-scale times a velocity-scale of SGS motions. The length-scale is clearly related to the grid (or filter) scale. Mason (1994) argues that the filter scale should be considerably larger than the grid scale in order to avoid numerical approximation errors. The velocity scale is often approximated by the magnitude of the velocity deformation (Smagorinsky 1963; Deardorff 1970) or the square-root of the turbulent energy of subgrid-scale motions (Lilly 1967; Schumann 1975). As first shown by Lilly (1967), the mean magnitude of the eddy viscosity can be evaluated from the inertial range energy spectrum when the grid-scale is well within the inertial subrange. All these models align the stresses with the velocity deformation, and, therefore, are absolutely dissipative. Such models were used successfully for LES of various turbulent flows. For reviews see Reynolds (1990) and Mason (1994). It is common opinion that the details of the model are of minor importance once the grid scale is small compared to the main energy carrying motion scales, and this has been supported by comparing the results of various LES models

with different SGS models for isotropic turbulence (see Métais & Lesieur 1992), and for convective boundary layer flows (Nieuwstadt *et al.* 1993).

However, in recent years, several problems with such models were identified. Clark *et al.* (1979) analysed results from direct numerical simulation of isotropic turbulence at moderate Reynolds number, $Re_\lambda = u'\lambda/\nu \cong 30$ (u' is the root-mean-square turbulence velocity, λ is Taylor's microscale, and ν is the viscosity). In contrast to what the Smagorinsky–Lilly model assumes, they found that the actual SGS stresses are only weakly correlated with the local strain rates (the deformation tensor of the velocity field). This finding has been supported by several further analyses of simulated turbulence (Bardina *et al.* 1980; Horiuti 1989; Härtel & Kleiser 1992). Domaradzki *et al.* (1993), from numerical results for isotropic turbulence at $Re_\lambda = O(100)$, analysed a 20% correlation between SGS energy transfer and the large-scale dissipation ($\sim$ square of the strain rate tensor). Recently, Meneveau (1994) tested three versions of eddy-viscosity models including the usual Smagorinsky and the Lilly versions using (single-component) measurements of turbulence at $Re_\lambda \cong 170$. In agreement with the numerical analysis, he found that the correlation coefficient between the measured and modelled SGS stresses is small and in between 0.1 and 0.3. Smaller correlation values are found when using a cut-off filter, greater for top-hat and the greatest for Gaussian filters. He also found that the correlation depends on Δ/η, where $\eta = (\nu^3/\epsilon)^{1/4}$ is the Kolmogorov scale, and the differences between the correlations for various filters increases with decreasing value of Δ/η, but he gives no explanation for these trends. In an attempt to improve SGS models, Lund & Novikov (1992) related the stresses not only to the deformation but also to the rotation tensor and products thereof. However, the correlation between modelled and analysed stresses grows only a few percent by such expansions. This paper shows that such a low correlation is unavoidable due to random SGS motions.

The energy exchange between large- and small-scale motions can be computed from spectral closure models, such as the eddy-damped quasi-normal Markovian (EDQNM) theory, developed by Orszag (1970), Kraichnan (1976), Leslie & Quarini (1979), Herring *et al.* (1982), and Lesieur (1993). Some approximate results of this model are summarized in the appendix. These theories show that the energy exchange between grid-scale and subgrid-scale motions is not unidirectional. Energy is exchanged both from the large scales to the small scales and vice versa. The latter is called the backscatter of energy (Leslie & Quarini 1979). It is also responsible for the transfer of errors from small to large scales, limiting predictability (Chasnov 1991). Backscatter is caused by the triple interaction of two subgrid scales with a resolved scale. For wavenumbers k much smaller than the cut-off wavenumber $k_c \cong \pi/\Delta$, backscatter excites energy at the resolved scales at a rate increasing with k^4. This is the reason for a corresponding energy spectrum at small wavenumbers. Hence, backscatter excites mainly the smallest resolved motion scales. The contribution from subgrid scale motions to backscatter decreases with k^{-6} in the inertial subrange. Thus, only those motions scales which are a little bit smaller than the grid scale contribute to backscatter. Leslie & Quarini (1979) analysed the rate of backscatter for various filters and showed that the rate of backscatter in the inertial subrange scales with the dissipation rate. The rate of backscatter is strongest and amounts to $B = 1.37\epsilon$ for a sharp cut-off filter. It gets strongly reduced when the sharp filter is replaced by a more smooth filter, such as a top-hat filter and a Gaussian filter, for which the rate of backscatter reduces to 0.489 and 0.340ϵ. For sharp filters, both the backscatter and the drainage of energy from small to large wavenumbers show large cusps near

the cut-off wavenumber. The cusps get smoothed when the inertial range spectrum is replaced by a more realistic spectrum with zero energy at low wavenumbers. Also smooth filters do not cause such cusps so that a spectrally uniform eddy diffusivity may be used with such filters.

From numerical analysis of direct numerical simulations of channel flows, Piomelli *et al.* (1991) showed that the local energy exchange between large and small scales can nearly as often be backwards as forward and the local rate of backscatter may be considerably larger than the net rate of energy dissipation ϵ. Domaradzki *et al.* (1993, 1994) confirmed these findings for isotropic turbulence, for turbulent shear flows, and for turbulent convection between plane walls. They showed that the exchange of energy between resolved and subgrid scales is carried mainly by motions at wavenumbers within one half and twice the cut-off wavenumber. Possibly due to limited Reynolds number, these flow simulations exhibit mean backscatter which is of a magnitude comparable to the mean energy drain at large scales but reaches only about 15% of that drain at the smallest resolved scales. Hence, the amount of backscatter depends on the flow details but backscatter is important and should be included in SGS models for realistic LES of turbulence.

Bardina *et al.* (1980) introduced an improved SGS model which combines the Smagorinsky model with a model based on the stresses at the smallest resolved scales. This model gives higher correlations (about 0.5) than the Smagorinsky model between modelled and analysed SGS stresses (Horiuti 1989). Since the stresses are no longer strictly aligned with the velocity deformation tensor in their model, backscatter may occur. Leonhard (1974) identified stress contributions from interactions between filtered velocities causing forward scatter for smooth filters. Antonopoulos-Domis (1981) found in numerical tests that these Leonard-stresses have small consequences for the decay rate of isotropic turbulence. Interactions between resolved and subgrid-scales motions, the so-called cross-stresses, induce backscatter (Horiuti 1989) balancing most of the forward scatter due to the Leonard stresses. Germano (1992) and Germano *et al.* (1991) proposed a so-called 'dynamical' extension of the Smagorinsky model in which the model coefficient is computed so that the stresses at subgrid scales dissipate energy at the same rate as the stresses at the smallest resolved scales, either locally or in some mean, again with considerable improvements. This model allows for partial backscatter of energy in regions of reduced eddy viscosity. Strong backscatter would require negative viscosity but that leads to numerically unstable solutions. Ghosal *et al.* (1992) tested various variants of the dynamical model but found that the results in terms of spectra and decay rates are only weakly sensitive to such model variations. All these models are deterministic functions of the resolved fields, and, hence, miss to represent the stochastic nature of backscatter.

Bertoglio (1985) and Chasnov (1991) included white-noise random forcings in LES of homogeneous turbulence to account for backscatter effects. They adjusted the amplitude of the forcing such that the resultant rate of backscatter corresponds to that predicted by the EDQNM. By this adjustment the forcing looses any relationship to realizable SGS stresses, and Bertoglio (1985) noted that the simulation of backscatter by a white-noise process (where the forcings at two successive time steps are uncorrelated) is rather unphysical. He compared forcings with zero and finite temporal correlation. Both gave small differences for second-order statistics but cause different third-order correlations. These spectral models are well suited for homogeneous turbulence but difficult to apply for more complex flows.

Recently, Leith (1990) and Mason & Thomson (1992) (abbreviated as MT) introduced more simple but also more heuristic methods to simulate stochastic backscatter in non-homogeneous flows. They add random forces (or heat sources) to the equations of motion. The random forces are specified in terms of the rotation of a random vector potential in order to eliminate stochastic contributions to pressure fluctuations; the divergence of a random flux vector is used as stochastic heat source. The random forcing was smoothed spatially with a filter to avoid large numerical truncation errors. In time, their forcing represents a white-noise process. MT changed the forcing after each second time-step of the numerical integration scheme. The amplitude of the forcing is determined on dimensional arguments by Leith (1990). MT consider random stresses and fluxes and derive a rough estimate of the rate of backscatter for kinetic energy which agrees with EDQNM computations of Chasnov (1991) and Leslie & Quarini (1979). The backscatter of temperature variances is estimated by MT using EDQNM approximations as described in the appendix. These estimates were used by MT to adjust the amplitude of the forcing.

Leith showed that backscatter may excite turbulence in a two-dimensional simulation of a shear flow. MT investigated a boundary layer shear flow near rigid walls. They pointed out that simulations with the usual Smagorinsky model (and with various length-scale assumptions) result in mean velocity profiles which deviate from the logarithmic form expected near surfaces. They showed that the mean shear in a LES with stochastic forcing agrees better with the expected uniform value. Moreover, the stochastic forcing causes more small-scale turbulence with reduced anisotropy near walls in better agreement with observations. Their work is to be regarded as an essential step forward in our understanding of the importance of stochastic forcing for shear flows. It is, however, not yet clear whether stochastic forcing is the only mean to ensure the correct velocity profile. In fact, Sullivan *et al.* (1994), who extended an earlier proposal by Schumann (1975) with a splitting of the SGS stresses into a fluctuating and a mean part, using different models for the different stresses, obtained the expected logarithmic profile without stochastic forcing. Horiuti (1989) and Härtel & Kleiser (1992) found systematic negative correlations between stress and strain rate fluctuations near walls suggesting that backscatter in such regions is caused by coherent motion structures which cannot be approximated by random motion models. Andrén *et al.* (1994) applied various LES models to the Ekman boundary layer showing again the strong impact of stochastic forcing. They find, however, that improvement with respect to the degree of anisotropy near walls may also be obtained with reduced eddy viscosity. Anyway, the work of MT, and its refinements and applications (Mason 1994; Mason & Brown 1994), demonstrates the importance of stochastic forcing. None of these models explains the observed weak correlations between stresses and strain rates (or fluxes and scalar gradients). In the following section, we introduce a simple stochastic SGS model which resembles explicitly the random nature of the SGS stresses and fluxes.

3. A random subgrid-scale model

(*a*) *Random subgrid-scale fluxes*

As in Reynolds (1895), mean values or filtered fields are denoted by bars and fluctuations by primes, and the mean or filter represents an average over the surroundings of the position under consideration. Ensemble mean values (mean-mean values in the

sense of Reynolds 1895) will be denoted by angular brackets. The precise details of the filter will not be taken into account. Actually, the filter is implemented by the discrete representation of the flow field on the finite-difference grid. For approximate analysis, one may assume that this represents a top-hat filter which averages over a grid cell. However, details of the finite-difference implementation of differences and interpolations will affect the effective filter. Formally, the SGS stresses and fluxes are defined by

$$\overline{u_i' u_j'} \equiv \overline{u_i u_j} - \overline{u_i}\,\overline{u_j}, \quad \overline{u_i' T'} \equiv \overline{u_i T} - \overline{u_i}\,\overline{T}. \tag{3.1}$$

Here, u_i and T denote the Cartesian velocity components and the temperature (or any other scalar) field. As shown by Leonard (1974) and Germano (1992), stresses are not equal to the mean values of products of fluctuating quantities, but composed of various terms including interactions between the SGS motions and the resolved motions (such as the Leonard stresses). We do not distinguish between these components but model them together.

The classical Smagorinsky–Lilly model relates the SGS stresses and fluxes with the strain rate tensor of the resolved (or filtered) velocity field and the gradients of the resolved scalar field

$$\bar{D}_{ij} = \frac{\partial \bar{u}_i}{\partial x_j} + \frac{\partial \bar{u}_j}{\partial x_i}, \quad \bar{D}_{iT} = \frac{\partial \bar{T}}{\partial x_i}, \tag{3.2}$$

using SGS eddy diffusivities K_m and K_h for momentum and heat,

$$\overline{u_i' u_j'} = -K_\mathrm{m} \bar{D}_{ij} + \tfrac{2}{3}\delta_{ij} e, \quad \overline{u_i' T'} = -K_\mathrm{h} \bar{D}_{iT}. \tag{3.3}$$

The SGS kinetic energy,

$$e = \tfrac{1}{2}\overline{u_i'^2}, \tag{3.4}$$

is added isotropically to the stresses to ensure non-zero variances for incompressible flows in which $\bar{D}_{ii} = 0$. For constant diffusivities, this model implies a 100% correlation between stresses and strain rates. Hence, the model is purely dissipative and free of stochastic contributions.

In order to represent stochastic effects, we assume that parts of the SGS motions behave as random fields with wavelengths smaller than the grid scale Δ, and with timescales which are proportional to the turn-over time of SGS motions $\Delta/e^{1/2}$. Part of the stresses are related to the mean gradients as given by the above model, the other part is assumed to be due to SGS motions which do not correlate with the mean gradients. Hence, we consider the weak correlation between stresses and strain rates to be of physical nature. We will see (in § 3 *b*) that such stresses out of phase with the strain rates induce random forces and cause backscatter when properly correlated in time. Hence, the random forcing enters the equations as a natural consequence of random stresses.

The random fluxes are caused by SGS motions which are more isotropic than the resolved fields. Therefore, we assume that random stresses R_{ij} and random fluxes q_i add isotropically to the deterministic model parts,

$$\overline{u_i' u_j'} = -K_\mathrm{m} \bar{D}_{ij} + \tfrac{2}{3}\delta_{ij} e + R_{ij}, \quad \overline{u_i' T'} = -K_\mathrm{h} \bar{D}_{iT} + q_i, \tag{3.5}$$

with zero ensemble mean values,

$$\langle R_{ij} \rangle = 0, \quad \langle q_i \rangle = 0. \tag{3.6}$$

By its definition, the SGS stress is a positive definite tensor, regardless of the mean

field gradients, and this should be reflected by the model for realizability (Schumann 1977).

The fluctuating fluxes are modelled as if they were caused by fluctuating velocities v_i and fluctuating temperature fields θ, with zero ensemble mean, defined for each grid point, such that

$$R_{ij} = \gamma_{\mathrm{m}}(v_i v_j - \tfrac{2}{3}\delta_{ij}e), \quad q_i = \gamma_{\mathrm{h}} v_i \theta, \quad 0 \leqslant \gamma \leqslant 1, \quad \text{for} \quad \gamma = \gamma_{\mathrm{m}}, \gamma_{\mathrm{h}}. \tag{3.7}$$

By definition, these quadratic expressions provide positive definite Reynolds stresses and realizable heat fluxes with zero mean for those parts which are independent of the resolved gradients. Here, the coefficients γ (γ_{m} and γ_{h}) are yet free model parameters, in between 0 and 1, which determine the fraction of randomness affecting the SGS fluxes.

The fluctuating fields are constructed from random number fields Z_i and Z_T. For consistency with the original definitions of SGS fluxes, the amplitudes have to be functions of the SGS kinetic energy e and half the SGS temperature variance $e_T \equiv \frac{1}{2}\overline{T'^2}$,

$$v_i = (2e/3)^{1/2} Z_i, \quad \theta = (2e_T)^{1/2} Z_T. \tag{3.8}$$

The random numbers Z_i represent a white-noise process in space on the grid with positions $\boldsymbol{x}$. In time t the random numbers correlate at timescales τ_v for velocity fields and τ_θ for temperature. Hence, the random numbers are generated with ensemble mean properties,

$$\langle Z_i \rangle = 0, \tag{3.9}$$

$$\langle Z_i(\boldsymbol{x}, t) Z_j(\boldsymbol{x}', t') \rangle = \delta_{ij}\delta_{\boldsymbol{x}\boldsymbol{x}'} \exp(|t - t'|/\tau), \tag{3.10}$$

i.e. unit variances but zero cross-correlations, for $i, j = 1, 2, 3, T$. As a consequence of these definitions, the resultant stresses and fluxes satisfy equation (3.6) The correlations decay in time with a timescale $\tau = \tau_v$, for $i \leqslant 3$, and $\tau = \tau_\theta$, for $i = T$. The random stresses and fluxes are Galilean invariant, as necessary, because they depend only on velocity fluctuations. This also requires that the timescales are understood in the Lagrangian sense (and implemented this way, see § 4 *d*). It is plausible to relate them to the turn-over time of the SGS motion fields. For passive scalar, the equations are linear in temperature, therefore the timescale of temperature is related to that for velocity. For high Reynolds and Péclet numbers, it is reasonable, therefore, to assume

$$\tau_v e^{1/2}/\Delta = c_{\tau v}, \quad \tau_\theta e^{1/2}/\Delta = c_{\tau\theta}, \tag{3.11}$$

with coefficients $c_{\tau v}$ and $c_{\tau\theta}$ of order one.

For incompressible flows, the fluctuating fields v_i should satisfy continuity,

$$\delta_i v_i = 0, \tag{3.12}$$

where the operator δ_i denotes a finite difference approximation to the spatial derivative in the i-direction on the discrete grid. In principle, this can be achieved in various ways, e.g. by correcting with the gradient of a potential ϕ, which is computed just as the pressure field in the LES under the constraint that v_i satisfies equation (3.12). Alternatively, one might construct v_i as the rotation of other vector fields (but this gives the wrong backscatter spectrum, see § 4 *a*).

For simplicity we assume that the random fields have Gaussian probability density functions. This would be fully appropriate if the motion fields v_i and θ would represent the integral effects of a large number of independent random SGS motions.

Previous examinations of the Gaussian properties of turbulent velocities (Schumann & Patterson 1978; Métais & Lesieur 1992) showed that the assumption of Gaussian velocity and temperature fields is not completely unrealistic, but velocity differences and higher order moments of the velocities deviate from Gaussian behaviour in real turbulence because of energy transfer by third-order interactions, damping of third-order moments by non-zero fourth-order cumulants (Orszag 1970), and possibly intermittent variations. The assumption of Gaussian fields is fully consistent with the quasi-normal approximation used to express fourth-order correlations as a function of second-order ones in statistical theories like the EDQNM method (Orszag 1970). Borgas & Sawford (1994) constructed random forces with intermittency to simulate turbulent dispersion of particles. They found small effects of such intermittency compared with the dispersion by Gaussian forcing. The nonlinear acceleration term of the Navier–Stokes equations has been shown to be less intermittent with smaller variance than expected for Gaussian fields (Chen *et al.* 1989).

The random fields v_i and θ are constructed to approximate the velocity and temperature fields at wavelengths Δ, i.e. such that they represent the longest unresolved motion components. In principle, the random fields should represent a sum of random Fourier components at all wavenumbers higher than the cut-off wavenumber with decreasing amplitudes and timescales (see Kraichnan 1976; Bertoglio 1985). However, as shown by EDQNM results (see the appendix) and by the data of Domaradzki *et al.* (1993), the smaller scales contribute very little to backscatter. The coefficients γ determine the fraction of SGS motions contributing to random fluxes. For a rough estimate, let us assume that only the motions at scales in between the maximum resolved wavenumber $k_c \cong \pi/\Delta$, and nk_c contribute to random fluxes. Within the inertial range, where the spectra follow a $k^{-5/3}$ law, the related fraction of energy variance might be estimated to be given as

$$\gamma^2 = \int_{k_c}^{nk_c} k^{-2m}\,\mathrm{d}k \Big/ \int_{k_c}^{\infty} k^{-2m}\,\mathrm{d}k = 1 - n^{1-2m}. \tag{3.13}$$

i.e. $\gamma = 0.90$ for $n = 2$ and $m = 5/3$. This suggests that γ is a little less than one. However, as explained in the appendix, contributions from SGS motions to backscatter decrease more strongly because of variable timescales, $\vartheta_{0pp}E^2(k)k^{-2} \sim k^{-6}$. Thus $\gamma^2 = 1 - n^{-5}$ is close to one for any realistic value of n.

The coefficients γ could be computed from measured stresses and fluxes, if available, by requiring that measured variances of random stresses and fluxes, R_{ij} and q_i, are the same as the modelled terms in the ensemble mean, i.e.

$$\gamma_{\mathrm{m}}^2 = \langle R_{ij}^2\rangle / \langle [v_i v_j - \tfrac{2}{3}\delta_{ij}e]^2\rangle, \quad \gamma_{\mathrm{h}}^2 = \langle q_i^2\rangle / \langle (v_i\theta)^2\rangle. \tag{3.14}$$

By means of Schwarz's inequality one finds that these ratios are smaller than one for realizable stresses and fluxes. The proper values of γ will be discussed further in § 3 *d* and § 4 *c*.

The model is to be completed by equations to predict e and e_T using proper budget equations and diffusivities K_{m} and K_{h} as described in Schmidt & Schumann (1989). Before discussing these equations, which is done in § 4 *b*, we estimate the rates of backscatter of energy and variance.

(*b*) *Mean rate of stochastic backscatter for arbitrary forcing*

Any random stresses and fluxes induce random accelerations r_i and heat sources r_T,

$$r_i = -\delta_j R_{ij} - \delta_i p, \quad r_T = -\delta_i q_i, \tag{3.15}$$

where the former are modified by the induced stochastic pressure fluctuations p for continuity (our notation assumes unit density),

$$\delta_i r_i = 0. \tag{3.16}$$

As a consequence, the stochastic pressure force is the solution of a Poisson equation,

$$\delta_i \delta_i p = -\delta_i \delta_j R_{ij}. \tag{3.17}$$

Any isotropic part of the stresses, such as $(1-\gamma_\mathrm{m})\frac{2}{3}\delta_{ij}e$, only changes the pressure but does not contribute to the random acceleration.

At this stage, our model is basically very similar to those of Leith (1990) and MT. As in their approach, we have a random solenoidal force representing a white-noise Gaussian process. But we impose finite memory and our forcing is limited in magnitude by the amplitude of the random velocity fields. The forcing cannot be larger than for the cases with $\gamma = 1$. This limitation is purely of kinematical nature. Only the timescales require a dynamical model. As a more pragmatic aspect, we note that the present theory uses only four random fields Z_i, whereas MT use two more random fields to specify the random heat source as the divergence of a random vector.

The random forces (temperature sources) transfer kinetic energy $E = \frac{1}{2}\bar{u}_i^2$ (half temperature variance $E_T = \frac{1}{2}\bar{T}^2$) from the SGS motions to the resolved motion scales at rates,

$$B = r_i \bar{u}_i, \quad B_T = r_T \bar{T}, \tag{3.18}$$

and hence describe the backscatter process. The correlations between the random forces and the resolved motions depend on the flow-history. A precise analysis of this is as difficult as the turbulent flow prediction. It requires knowledge of Green's functions relating unit force impulses in the past with the resultant flow changes at the time and space point under consideration. Such Green's functions depend nonlinearly on the past flow field (Orszag 1970; Kraichnan 1976). Since we don't know these functions, we use an approximation neglecting all other history effects except the random forcing. In this approximation the actual resolved velocities and temperatures are Lagrangian time-integrals over the past forcing, e.g.

$$\bar{u}_i(t) = \int_{-\infty}^{t} r_i(t')\,\mathrm{d}t'.$$

We also note that in the ensemble mean, for a stationary process with constant timescales,

$$\langle r_i(t) r_i(t')\rangle = \gamma_\mathrm{m}^2 \langle \delta_\mathrm{m}[v_\mathrm{m}(t) v_i(t)]\delta_n[v_n(t') v_i(t')]\rangle = \langle r_i(t)^2\rangle \mathrm{e}^{-2(t-t')/\tau_v}, \tag{3.19}$$

and

$$\langle r_T(t) r_T(t')\rangle = \gamma_\mathrm{h}^2 \langle \delta_i[v_i(t)\theta(t)]\delta_j[v_j(t')\theta(t')]\rangle = \langle r_T(t)^2\rangle \mathrm{e}^{-(t-t')/\tau_v - (t-t')/\tau_\theta}. \tag{3.20}$$

Therefore, the ensemble mean rate of energy backscatter is

$$\langle B\rangle = \left\langle r_i(t)\int_{-\infty}^{t} r_i(t')\,\mathrm{d}t'\right\rangle = \langle r_i^2(t)\rangle\int_{-\infty}^{t}\mathrm{e}^{-2(t-t')/\tau}\,\mathrm{d}t' = \tfrac{1}{2}\tau\langle r_i^2\rangle, \tag{3.21}$$

with $\tau = \tau_v$ and a factor 2 because the forces depend on the square of the random velocity fields. Hence, stresses decorrelate more quickly than velocities. The ensemble mean rate of backscatter of temperature variance

$$\langle B_T\rangle = \langle r_T^2(t)\rangle\int_{-\infty}^{t}\mathrm{e}^{-(t-t')(1/\tau_v+1/\tau_\theta)}\,\mathrm{d}t' = \tfrac{1}{2}\tau_\mathrm{h}\langle r_T^2\rangle \tag{3.22}$$

depends on the timescale $\frac{1}{2}\tau_\mathrm{h} = (\tau_v^{-1}+\tau_\theta^{-1})^{-1}$ of heat fluxes. If corresponding measurements would be available, the timescales could be evaluated from

$$\tau = 2\langle r_i\bar{u}_i\rangle/\langle r_i^2\rangle, \quad \tau_\mathrm{h} = 2\langle r_\mathrm{h}\bar{T}\rangle/\langle r_\mathrm{h}^2\rangle. \tag{3.23}$$

The selection of the timescale values will be discussed further in § 3 *d*.

(*c*) *Mean rate of stochastic backscatter due to the random stresses*

In this section, we evaluate the rates of backscatter due to the given random stresses and fluxes by inserting equations (3.15), (3.7) and (3.8) into equations (3.21) and (3.22). For analysis, we assume locally isotropic and homogeneous flows with equal grid spacings Δ, in all three spatial coordinates. For homogeneous turbulence and using equation (3.17) one can show that the stochastic part of the pressure gradient reduces the backscatter according to

$$\langle B\rangle = \tfrac{1}{2}\tau\langle(\delta_j R_{ij})^2 - (\delta_i p)^2\rangle. \tag{3.24}$$

However, further analysis is difficult because of the spatial correlations induced by the pressure forces. Therefore, we evaluate these rates first analytically omitting the changes introduced by the pressure part and also neglecting the requirement of v_i satisfying continuity. Later, the rates are computed numerically without these simplifications and the results are expressed as a function of the analytical terms with some numerical correction factors ψ_m and ψ_h. In the first approximation, one obtains

$$\langle B\rangle = \tfrac{1}{2}\gamma_\mathrm{m}^2\langle[\delta_j(Z_iZ_j)]^2\rangle\langle\tau(2e/3)^2\rangle, \quad \langle B_T\rangle = \tfrac{1}{2}\gamma_\mathrm{h}^2\langle[\delta_i(Z_iZ_T)]^2\rangle\langle\tau_\mathrm{h}(2e/3)(2e_T)\rangle. \tag{3.25}$$

From now on, we assume that the SGS energies and timescales are smooth fields such that $\tau \cong$ const., and $\langle e^2\rangle \cong \langle e\rangle^2$, and similarly for e_T. From LES results for e this has been found to be valid up to errors less than about 10% (Schumann 1975), and this finding has been confirmed in the tests which will be described in § 4 *d*. We see that the backscatter rates are controlled by the squared gradients of the random numbers. For isotropic and spatially uncorrelated random fields one obtains

$$\langle[\delta_j(Z_iZ_j)]^2\rangle = 3\langle[\delta_1(Z_1Z_1)]^2\rangle + 6\langle[\delta_2(Z_1Z_2)]^2\rangle = 6\Delta^{-2}(\langle Z_1^4\rangle + \langle Z_1^2\rangle^2) = 6(F+1)\Delta^{-2}, \tag{3.26}$$

$$\langle[\delta_i(Z_iZ_T)]^2\rangle = 3\langle[\delta_1(Z_1Z_T)]^2\rangle = 6\Delta^{-2}\langle Z_1^2\rangle\langle Z_T^2\rangle = 6\Delta^{-2}. \tag{3.27}$$

These terms comprise fourth-order velocity moments so that the flatness factor $F \equiv \langle Z_1^4\rangle/\langle Z_1^2\rangle^2$ influences the backscatter of kinetic energy. The backscatter of temperature variance depends only on second-order moments in this model with independent random velocity and temperature fields. For Gaussian random fields, the

Table 1. *Coefficients of the backscatter model in cases with local evaluation (a to d) and with averaging according to second-order finite differences (A to D)*

(For cases c and C, solenoidal fields v_i are generated using a pseudo pressure-potential. For cases d and D, the solenoidal fields v_i are computed from rotation of a random vector potential. Listed are the stochastic r.m.s. pressure fluctuations relative to the SGS kinetic energy e for unit density, and ψ_m and ψ_h, the coefficients of equations (3.28). Given are the mean values and their statistical uncertainties.)

case	$\delta_i v_i = 0$	$\delta_i r_i = 0$	$\langle p^2\rangle^{1/2}/(\gamma_\mathrm{m}^2\langle e\rangle)$	ψ_m	ψ_h
a	no	no	0	1 ± 0.01	1 ± 0.01
b	no	yes	1.415 ± 0.008	0.5 ± 0.004	1 ± 0.01
c	yes	yes	1.193 ± 0.004	0.44 ± 0.003	0.8 ± 0.005
d	yes	yes	1.29 ± 0.006	0.47 ± 0.002	0.755 ± 0.005
A	no	no	0	0.223 ± 0.002	0.5 ± 0.004
B	no	yes	0.670 ± 0.003	0.112 ± 0.001	0.5 ± 0.004
C	yes	yes	0.481 ± 0.003	0.0775 ± 0.0004	0.25 ± 0.002
D	yes	yes	0.463 ± 0.002	0.0643 ± 0.0006	0.25 ± 0.002

flatness factor amounts to $F = 3$. For strongly intermittent fields with exponential distributions (Métais & Lesieur 1987) one has $F = 6$, implying stronger rates of backscatter. Smaller backscatter results if the random numbers were taken from a standard pseudo-random number-generator with equal distribution within a finite interval, where $F = 9/5$. Here, $F = 3$ is assumed for a first approximation.

For the complete model, including the continuity constraints for v_i and r_i according to equations (3.12) and (3.16), the backscatter rates have to be evaluated from equations (3.21) and (3.22) using the given definitions for the random forcings. This has been done numerically and the results are expressed as

$$\langle B\rangle = [\tfrac{4}{3}(F+1)]\gamma_\mathrm{m}^2\psi_\mathrm{m}\langle e\rangle^2\tau/\Delta^2, \quad \langle B_T\rangle = 4\gamma_\mathrm{h}^2\psi_\mathrm{h}\langle e\rangle\langle e_T\rangle\tau_\mathrm{h}/\Delta^2. \tag{3.28}$$

Dimensionally, these results are fully consistent with the EDQNM results as given in equation (A 3) of the appendix and also with MT's estimates. The correction factors ψ_m and ψ_h would be unity in the above simplified analysis for Gaussian random numbers. The numerical analysis has been performed generating Gaussian fields Z_i from a pseudo-random number-generator. The fields v_i and θ are computed thereof with arbitrary constant values of e and e_T. The random fields v_i are then adjusted to continuity by using their divergence as input for a direct solver of a Poisson equation (Schumann & Sweet 1988) to obtain a pseudo-pressure-potential ϕ. After subtraction of the gradient of this potential, one obtains solenoidal fields v_i satisfying equation (3.12). These fields are used to construct the random fluxes, equation (3.7). In computing the random forces, again a Poisson equation, equation (3.17) is solved to obtain the stochastic part of the pressure p. By various tests it has been found that the results are grid independent and achieve sufficient statistical significance for a grid with 32^3 grid points and 10 realizations.

If the finite differences are computed as compact as possible on the discrete grid, avoiding any spatial averaging, one obtains the results listed in rows a–d of table

1. Row a contains the results without any correction for continuity, row b lists the results if the correction $\delta_i\phi$ to v_i is neglected but including the effect of the pressure p according to equation (3.15), and row c lists the results of the complete model. Row d gives the values if the velocities v_i are computed as the rotation of the random numbers Z_i, $i = 1, 2, 3$. We see that the numerical data give unit correction factors for the case without any continuity constraints, with a statistical uncertainty of 1%. This confirms the given analysis. Moreover, we find that the continuity condition reduces the backscatter of kinetic energy by $\psi_\mathrm{m} \cong 0.44$, and that of temperature variance by $\psi_\mathrm{h} \cong 0.8$. The root-mean square value of the stochastic pressure is about $1.2\gamma_\mathrm{m}^2\langle e\rangle$.

Up to now, we have evaluated the forcing assuming finite differences of the random fluxes without any filtering and without any averaging in space. However, in standard second-order finite-difference schemes on a staggered grid, as, for example, in Deardorff (1970), fluxes are computed from discrete approximations with spatial averages over neighbouring grid points. For consistency, in such a scheme one may approximate the random fluxes as

$$R_{ij} = \gamma_\mathrm{m}\,(\bar{v}_i^j\bar{v}_j^i - \tfrac{2}{3}\delta_{ij}\overline{\bar{e}^i}^j), \quad q_i = \gamma_\mathrm{h} v_i \bar{\theta}^i, \tag{3.29}$$

where the bars with post-superscripts denote algebraic mean values over adjacent grid points in the corresponding direction. In the same way, the scalar products are implemented as $\overline{(v_i^2)}^i$, and $\overline{(r_i^2)}^i$. The averaging on the grid implies a numerical filter which reduces the random forcing magnitude. For such approximations, the numerical values of the coefficients are given by rows A–D instead of a–d of table 1. We see that the numerical filter reduces backscatter of temperature variance by a factor 2 and backscatter of kinetic energy by about a factor 4.

(*d*) *Mean rate of stochastic backscatter in the inertial subrange*

It remains to relate the rate of backscatter to the rate of dissipation ϵ of kinetic energy and the rate of molecular destruction of half the temperature variance ϵ_T. For grid scales Δ within the inertial subrange of turbulence, both 'dissipation' rates can be estimated, as in Schmidt & Schumann (1989), from

$$\epsilon = c_\epsilon\langle e\rangle^{3/2}/\Delta, \quad \epsilon_T = c_{\epsilon T} > \langle e\rangle^{1/2}\langle e_T\rangle/\Delta, \tag{3.30}$$

with coefficients

$$c_\epsilon = \pi[2/(3\alpha)]^{3/2} = 0.845, \quad c_{\epsilon T} = \pi[2/(3\alpha)]^{1/2}2/(3\beta) = 2.02. \tag{3.31}$$

Here $\alpha = 1.6$ and $\beta = 0.67$ are the coefficients of the spectra of kinetic energy and half the temperature variance versus wavenumber k, $E(k) = \alpha\langle\epsilon\rangle^{2/3}k^{-5/3}$, $E_T(k) = \beta\langle\epsilon_T\rangle\langle\epsilon\rangle^{-1/3}k^{-5/3}$.

The timescales τ and τ_h are estimated using the EDQNM-result, equation (A 6) with (A 11) for $p = k_\mathrm{c} = \pi/\Delta$. We note, that τ and τ_h introduced in equations (3.21) and (3.22) actually denote half the relevant timescales. However, also θ_{0pp} and θ_{0pp}^T define half the timescales of the stresses and fluxes. This can be understood from the corresponding definitions given by, for example, Herring *et al.* (1982). Hence, we set

$$\tau = \theta_{0pp} = c_{\tau v}\Delta/e^{1/2}, \quad \tau_\mathrm{h} = \theta_{0pp}^T = c_{\tau h}\Delta/e^{1/2}, \tag{3.32}$$

$$c_{\tau v} = \frac{3^{1/2}1500}{2^{1/2}319\alpha^{3/2}\pi} = 0.906, \quad c_{\tau h} = \frac{3^{1/2}1500}{2^{1/2}1045\beta\alpha^{1/2}\pi} = 0.660. \tag{3.33}$$

The corresponding timescale for temperature is $\tau_\theta = (2/\tau_\mathrm{h} - 1/\tau_v)^{-1} = c_{\tau\theta}\Delta/e^{1/2}$, with $c_{\tau\theta} = 0.519$. These coefficients are of order one as expected. They show that temperature fluctuations, which are not constrained by the continuity condition, decorrelate more quickly than velocity.

From equations (3.28) and (3.30) we obtain

$$\langle B\rangle = \gamma_\mathrm{m}^2\psi_\mathrm{m}[\tfrac{4}{3}(F+1)](c_{\tau v}/c_\epsilon)\langle\epsilon\rangle, \quad \langle B_T\rangle = \gamma_\mathrm{h}^2\psi_\mathrm{h}4(c_{\tau h}/c_{\epsilon T})\langle\epsilon_T\rangle. \tag{3.34}$$

Since $c_{\tau v}/c_\epsilon = 3375/(319\pi^2)$, $c_{\tau h}/c_{\epsilon T} = 3375/(1045\pi^2)$, the rates of backscatter are independent of the values of α and β, consistent with the estimates given in equation (A 14). Finally, the present estimates $\psi_\mathrm{m} = 0.44$, $\psi_\mathrm{h} = 0.8$, $c_\epsilon = 0.845$, $c_{\epsilon_T} = 2.02$, $c_{\tau v} = 0.906$, $c_{\tau h} = 0.660$, $F = 3$, result in

$$\langle B\rangle = \gamma_\mathrm{m}^2 c_B\langle\epsilon\rangle, \quad \langle B_T\rangle = \gamma_\mathrm{h}^2 c_{BT}\langle\epsilon_T\rangle, \tag{3.35}$$

with

$$c_B = 2.52, \quad c_{BT} = 1.05. \tag{3.36}$$

A larger flatness factor increases c_B. In contrast, the backscatter of variances is independent of fourth-order moments in this model. Except for the uncertainty in the flatness factor, these results, for $\gamma = 1$, represent upper bounds for the expected backscatter rates because they neglect the filtering by finite-difference interpolations. If we take the smaller values $\psi_\mathrm{m} = 0.0755$, $\psi_\mathrm{h} = 0.25$, as appropriate in a consistent finite-difference scheme (row C of table 1), the values reduce to

$$c_B = 0.43, \quad c_{BT} = 0.33. \tag{3.37}$$

The largest uncertainty of these results stem from the timescale estimates which were possibly overestimated by using the non-local EDQNM approximation at the cut-off wavenumber. Also the flatness factor $F = 3$, though consistent with EDQNM, and the fractions of random motions γ are uncertain. For $\gamma_\mathrm{m} = 0.75$ and $\gamma_\mathrm{h} = 0.65$, the present results agree with the values $c_B = 1.37$ or 1.4 and $c_{BT} = 0.45$ given by Leslie & Quarini (1979) and MT. Our smaller result 0.43 for c_B is quite close to the value 0.489 given by Leslie & Quarini (1979) for the top-hat filter. This shows again the strong sensitivity to the numerical filter. As derived in the appendix, even smaller values $c_B = 0.176$, $c_{BT} = 0.077$ become effective according to EDQNM when the filter is so smooth that only the largest scales experience backscatter.

4. Consequences of backscatter

(*a*) *Spectra of backscatter and stochastic pressure*

Any white-noise signal Z_i with Dirac-type spatial autocorrelation possesses a 'flat' Fourier power spectrum with equal mean amplitudes for each Fourier mode (Gardiner 1983, pp. 15–19). Also products Z_iZ_j have a flat spectrum because such products have the same Dirac-type spatial correlation. In three dimensions, the number of Fourier modes grows with k^2, where k is the magnitude of the wavenumber vectors. Consequently, the Fourier spectrum $E_Z(k)$ of Z_iZ_j varies as k^2. Any derivative δ_i gives another factor of k. Hence, the spectrum $B(k)$ of backscatter, which is the power spectrum of $r_i \sim \delta_j(Z_iZ_j)$, is proportional to $B(k) \sim k^2E_Z(k) \sim k^4$. This agrees with the expectations from EDQNM theory (Leslie & Quarini 1979), see also equations (A 3) and (A 8).

With the same kind of arguments one finds that the power spectrum of the stochastic pressure fluctuations scales with k^2. These results have been verified by computing numerically the spectrum of random forcing and of the pressure fluctuations within the computations described in § 3 *c* to determine the factors ψ.

It should be noted that the random forcing in terms of the rotation or the gradient of random white-noise vector fields, as used by MT and Leith (1990), gives also the required k^4 behaviour of backscatter. Hence, the introduction of the rotation or gradient operation is important not only for continuity but also for spectral consistency. On the other hand, a k^6 spectrum results if the random velocity fields v_i are specified as the curl of a white-noise random vector field. This method cannot be recommended, therefore. Spatially smooth eddy viscosities affect the energy transfer spectrum as k^2. Hence, the correct backscatter spectrum cannot be simulated by reducing the eddy viscosity.

(*b*) *Diffusivities and the turbulent Prandtl number*

The SGS stresses and fluxes induce forces which exchange energy and variance between resolved and subgrid scales. Parts of the stresses and fluxes are aligned with the strains and gradients and transfer energy forward (for positive diffusivities) to the subgrid scales, therefore. The remaining random (or non-aligned) parts are responsible for the backscatter, i.e.

$$P - B = -\overline{u_i' u_j'} \tfrac{1}{2} \bar{D}_{ij}, \quad P_T - B_T = -\overline{u_i' T'} \bar{D}_{iT}, \tag{4.1}$$

with forward transports

$$P = K_\mathrm{m} \tfrac{1}{2} \bar{D}_{ij}^2, \quad P_T = K_\mathrm{h} \bar{D}_{iT}^2, \tag{4.2}$$

and mean backscatter rates as given in equation (3.35). As sketched in figure 1, the budgets of SGS energy and variance comprise

$$\frac{\mathrm{d}\langle e \rangle}{\mathrm{d}t} = \langle P - B - \epsilon \rangle, \quad \frac{\mathrm{d}\langle e_T \rangle}{\mathrm{d}t} = \langle P_T - B_T - \epsilon_T \rangle. \tag{4.3}$$

Diffusion terms are included in the numerical simulations as in Schmidt & Schumann (1989) but vanish in the ensemble mean for homogeneous turbulence. For stationary turbulence, the budgets give

$$\langle P \rangle = \langle B + \epsilon \rangle = (1 + \gamma_\mathrm{m}^2 c_B) \langle \epsilon \rangle, \quad \langle P_T \rangle = \langle B_T + \epsilon_T \rangle = (1 + \gamma_\mathrm{h}^2 c_{BT}) \langle \epsilon_T \rangle. \tag{4.4}$$

For the same resolved motion fields, the diffusivities K_m and K_h have to be greater in cases with simulated backscatter than without ($K_\mathrm{m0}, K_\mathrm{h0}$) by the same factors as given above for the production rates. As noted before by MT, these factors are different for momentum and scalar diffusion. Hence the effective turbulent Prandtl number of SGS diffusivities changes as a consequence of backscatter,

$$Pr_\mathrm{SGS} = \frac{K_\mathrm{m}}{K_\mathrm{h}} = \frac{K_\mathrm{m0}}{K_\mathrm{h0}} \frac{1 + \gamma_\mathrm{m}^2 c_B}{1 + \gamma_\mathrm{h}^2 c_{BT}}. \tag{4.5}$$

(Reynolds's analogy of heat and momentum transport implies a turbulent Prandtl number of one.) The turbulent Prandtl number increases from its value for zero backscatter by a factor 1.7 for $\gamma_\mathrm{m} = \gamma_\mathrm{h} = 1$, if c_B, c_{BT} are given by equation (3.36), but only by a factor of 1.07 for the alternative set (3.37). For small wavenumbers, the non-local EDQNM approximation implies an increase of the turbulent Prandtl number of only 1.09 (see appendix).

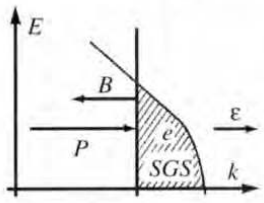

Figure 1. Sketch of the energy spectrum E versus wavenumber k (in logarithmic scales), illustrating the energy budget for SGS kinetic energy e at wavenumbers exceeding the cut-off wavenumber k_c, for given rates of production P, dissipation ϵ, and backscatter B of SGS kinetic energy.

All these results are yet independent of the model used for the SGS diffusivities,

$$K_m = c_m \Delta e^{1/2}, \quad K_h = c_h \Delta e^{1/2}. \tag{4.6}$$

As in Schmidt & Schumann (1989), the coefficients c_m and c_h are determined assuming equilibrium between production and dissipation, and evaluating the production terms from the integrals of $2K_m k^2 E(k)$ and $2K_h k^2 E_T$ from zero up to a cut-off wavenumber $k_c = \pi/\Delta$ for inertial range spectra. This results in

$$\langle P \rangle = \frac{c_m}{c_{m0}} \langle \epsilon \rangle, \quad c_{m0} = [2/(3alpha)]^{3/2}/\pi = 0.0856, \tag{4.7}$$

$$\langle P_T \rangle = \frac{c_h}{c_{h0}} \langle \epsilon_T \rangle, \quad c_{h0} = [2/(3alpha)]^{1/2} 2/(3\beta\pi) = 0.204, \tag{4.8}$$

with coefficients enlarged for backscatter as in equation (4.4),

$$c_m = c_{m0}(1 + \gamma_m^2 c_B), \quad c_h = c_{h0}(1 + \gamma_h^2 c_{BT}). \tag{4.9}$$

As a consequence, the turbulent Prandtl number amounts to $Pr_{SGS0} = \beta/\alpha = 0.42$ for zero backscatter. This value is rather small compared to observations and it is interesting that greater values get explained by backscatter. This has been noted before by MT who gave a similar analysis for the Smagorinsky model.

(*c*) *Correlations between stresses and strains*

As explained before, the classical Smagorinsky–Lilly model, for constant diffusivities, implies unit correlations between stresses and strain rates. On the other hand, we have shown that backscatter requires stresses which are not correlated with the strain rates. Therefore, the correlation between stresses and strain rates are smaller when the origin for backscatter is included. This reduction can be computed as follows.

As in Clark *et al.* (1979), we define the correlation coefficient $C_\tau = C(-\tau_{ij}, \bar{D}_{ij})$ between the (traceless) SGS stresses $\tau_{ij} \equiv \overline{u_i' u_j'} - \frac{2}{3} e \delta_{ij}$ and the strain rates $\bar{D}_{ij}$ as $C(a,b) = \langle ab \rangle / (\langle a^2 \rangle \langle b^2 \rangle)^{1/2}$ (with summation convention). This correlation contains terms like $-\tau_{ij} D_{ij} = 2P$, $D_{ij}^2 = 2P/K_m$, and $\tau_{ij}^2 = [-K_m D_{ij} + \gamma_m (v_i v_j - \frac{2}{3}\delta_{ij} e)]^2$. The mean square stresses can be evaluated analytically using non-solenoidal fields v_i and neglecting any averaging due to finite-difference approximations. Coefficients ψ_τ, ψ_q which correct for these approximations are computed as described in § 4 *b* and listed in table 2. Fortunately, the correction factors are essentially invariant with

Table 2. *Correction factors ψ_τ and ψ_q as used in equations (4.11)–(4.14) and resultant correlations C_τ and C_q for $\gamma_m = \gamma_h = 1$, for cases defined in table 1*

(The first of the given values for C_τ and C_q is computed from equation (4.13) and (4.14) with c_B and c_{BT} according to equation (3.34) and values of ψ_m and ψ_h as listed in table 1. The second value gives the correlations for $c_B = c_{BT} = 0$.)

case	$\delta_i v_i = 0$	ψ_τ	ψ_q	C_τ	C_q
a, b	no	1.0 ± 0.003	1.0 ± 0.003	0.74, 0.16	0.60, 0.31
c	yes	1.0 ± 0.005	1.0 ± 0.003	0.50, 0.16	0.55, 0.31
A, B	no	0.333 ± 0.002	0.505 ± 0.003	0.54, 0.27	0.60, 0.41
C	yes	0.356 ± 0.003	0.500 ± 0.003	0.35, 0.27	0.52, 0.41

respect to the continuity constraint for v_i. The result is

$$C_\tau = \frac{\langle P \rangle}{\langle K_m P + \psi_\tau \gamma_m^2 e^2 \tfrac{2}{3}(F+1)\rangle^{1/2} \langle P/K_m \rangle^{1/2}}. \tag{4.10}$$

This expression equals one for $\gamma_m = 0$, but gives smaller correlations for positive values of γ_m. In the inertial subrange, the shear production P, the diffusivity K_m, and the SGS energy e are related by equations (4.2), (4.6) and (3.30). Under the assumption that these fields are close to constants, one obtains

$$C_\tau \cong \left(1 + \frac{2(F+1)\psi_\tau \gamma_m^2}{3 c_{m0} c_\epsilon (1+\gamma_m^2 c_B)^2}\right)^{-1/2} = \left(1 + \frac{9(F+1)\psi_\tau \gamma_m^2 \alpha^3}{4(1+\gamma_m^2 c_B)^2}\right)^{-1/2} \leqslant 1. \tag{4.11}$$

We see that backscatter actually increases the correlation by increasing the production rate P and the diffusivities by the factor $c_m = c_{m0}(1 + \gamma_m^2 c_B)$. The correlations approach a minimum for weak backscatter ($c_B \to 0$) (e.g. because of small values of τ), for large random fractions of stresses ($\gamma_m \to 1$), for large flatness values F, and for fluxes computed from spatially averaged random fields (because of reduced backscatter). Table 2 compiles the correlations for various numerical representations of the fluxes.

Similarly, the correlation $C_q = C(-\overline{u_i' T'}, \bar{D}_{iT})$ between scalar fluxes and gradients amounts to

$$C_q = \frac{\langle P_T \rangle}{\langle K_h P_T + \psi_q \gamma_h^2 4 e e_T \rangle^{1/2} \langle P_T / K_h \rangle^{1/2}} \tag{4.12}$$

$$\cong \left(1 + \frac{4\psi_q \gamma_h^2}{c_{h0} c_{\epsilon T} (1+\gamma_h^2 c_{BT})^2}\right)^{-1/2} = \left(1 + \frac{27\psi_q \gamma_h^2 \alpha \beta^2}{2(1+\gamma_h^2 c_{BT})^2}\right)^{-1/2} \leqslant 1. \tag{4.13}$$

Again, the randomness of fluxes (measured by γ_h) reduces the correlation, backscatter c_{BT} increases it, but the flatness factor has no influence. The numerical averaging of the random velocities plays a smaller role for C_q than for C_τ (see table 2). Figure 2 depicts the correlations (for case c, i.e. for $\psi_\tau = \psi_q = 1$) for various parameter values. For $\gamma_m = \gamma_h = 1$, with and without backscatter, the correlations vary in between 0.16 and 0.50 for momentum and 0.31 and 0.55 for heat flux.

In the numerical tests of Clark *et al.* (1979), the correlation C_τ was found in between 0.27 and 0.37 using filtered isotropic flow simulation results at relatively

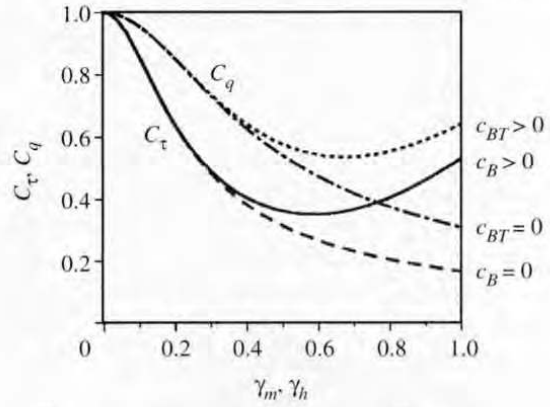

Figure 2. Correlation coefficients versus randomness coefficients γ_m or γ_h. Full curve: C_τ with backscatter ($\psi_\mathrm{m} = 0.44$), long-dashed, C_τ without backscatter ($\psi_\mathrm{m} = 0$). Short-dashed curve: C_q with backscatter ($\psi_\mathrm{h} = 0.8$), dash-dotted: C_q without backscatter ($\psi_\mathrm{h} = 0$).

low Reynolds number. Horiuti (1989) and Härtel & Kleiser (1992) found about the same values inside of a turbulent channel flow at comparable Reynolds numbers. It is an open question whether these correlations are larger or smaller at higher Reynolds numbers for flows with an inertial range. In view of equation (A 3), one should expect that the rate of backscatter is the larger the slower the energy spectrum decays at the smallest SGS wavenumbers. This suggests larger correlations C_τ in the inertial range than in the viscous range. On the other hand, Meneveau (1994) got lower values than Clark *et al.* (1979), in spite of relatively high Reynolds numbers.

Meneveau (1994) finds also smaller values of C_τ for data filtered with a cut-off filter than with a top-hat filter. For a top-hat filter, as for any other spectrally smooth filter, it appears reasonable that the SGS motions, which overlap in wavenumber space with the finest resolved motions, are correlated more strongly with the resolved motions. Therefore, the parameters γ should be smaller for a smooth filter than for the cut-off filter. For smaller values of γ, the above model gives larger correlations which may explain the observed trends. The filters will have larger effects for steeper spectral slopes. This explains perhaps the observed stronger sensitivity to filtering for Δ near the Kolmogorov scale compared to that for larger filter scales. The correlations of C_τ measured with smooth filters are of the order 0.3. For this value, figure 2 implies $\gamma_\mathrm{m} > 0.6$. For the cut-off filter and within the inertial subrange, the observed correlation value is 0.15, indicating $\gamma_\mathrm{m} \cong 1$. Unfortunately, no data are available on correlations C_q for heat fluxes, for which our theory suggests definitely larger correlations than for stresses.

(*d*) *Effect of backscatter in LES of decaying isotropic turbulence*

The modified SGS model with random stress components has been applied in a LES of decaying isotropic and isothermal turbulence. Although one expects, see MT, backscatter to be more important for shear flows near walls, we nevertheless consider here the much more simple case of isotropic decaying turbulence because of its well-known properties. Moreover, this test case is selected to get some experience with the new model at a modest amount of programming and computational work.

For that purpose, we adopt the LES version of a code developed by Kaltenbach *et al.* (1994) for simulation of homogeneous turbulence in a cube with periodic boundary conditions and second-order finite-differences on a staggered grid. Gerz & Palma

(1994) implemented the Smagorinsky–Lilly model with a transport equation for the SGS kinetic energy. The code had already three scalar fields implemented which we use in this application to store the random fields.

In any explicit numerical integration scheme the time step Δt will be limited for stability by the Courant criterion such that $\Delta t < \Delta/U$, where U is the maximum velocity in the computational domain. Since $e^{1/2} < U$, the time step will be usually much smaller than τ. In order to generate the proper temporal correlations, the random velocities v^n (the Cartesian index i is omitted for brevity) at each time step $t_n = n\Delta t$ are computed as a weighted sum of their values at the previous time step after being advected with the flow field, and independent random disturbances Z^n at each time step, using a Langevin-type equation,

$$v^n = v^{n-1}\left(1 - \frac{\Delta t}{\tau_v}\right) + \left[\frac{\Delta t}{\tau}\left(2 - \frac{\Delta t}{\tau}\right)\right]^{1/2} \sigma Z^n, n = 1, 2, \ldots, \tag{4.14}$$

with $\sigma^2 = \frac{2}{3}e$, $\tau \equiv \tau_v$, and $v^0 = \sigma Z^0$. This procedure results in random fields v^n with

$$\langle v^n \rangle = 0, \quad \langle (v^n)^2 \rangle = \sigma^2,$$

$$\langle v^n v^{n-i} \rangle = \sigma^2 (1 - \Delta t/\tau)^i \cong \sigma^2 \exp(-\mathrm{i}\Delta t/\tau), \quad \langle v^n v^{n-i} \rangle = \delta_{i,n-i} \quad \text{if} \quad \tau = \Delta t. \tag{4.15}$$

By means of advection of v with the flow field, one obtains the required Lagrangian autocorrelation with suitable Galilean invariance. One could also apply the pressure-correction scheme to these random velocities for continuity just as for the resolved velocity fields, but we did not so for these exploratory tests.

Other code changes concern the addition of the random stresses, equation (3.29), to the Smagorinsky–Lilly model. The rate of backscatter $B = \gamma_{\mathrm{m}}^2 c_B \epsilon$ is included as a loss term in the SGS energy budget in addition to dissipation, and the coefficient c_{m} is increased as given in equation (4.10). The model was applied for $\gamma_{\mathrm{m}} = \gamma_{\mathrm{h}} = 1$, and $c_B = 1.24$. This value results from using $\psi_{\mathrm{m}} = 0.112$ according to row B of table 1 and accounts for the spatial filtering with non-solenoidal random velocities v_i. The simulations start from random initial fields with an initial energy spectrum of the shape $E(k) \sim (k/k_p)^8 \exp(-4(k/k_p)^2)$, as also used by Métais & Lesieur (1992) and Chasnov (1991), and unit initial velocity variance, $u' = 1$. The domain size is $L = 1$, and the peak wavenumber k_p corresponds to a wavelength $\frac{1}{8}L$, giving an initial integral length-scale of $\ell/L = 0.0458$. Viscous transports are set to zero. The spatial grid comprises 64^3 grid points and the time step is set to $\Delta t = 0.05L/u'$. The same time step provides stable numerical solutions with and without random stresses. There was no need to further smooth the random fields. The integration is performed over 640 time steps, i.e. over 11.1 turn-over times.

The LES method is applied for four cases. The reference case uses diffusivities as described above for a filter scale Δ, and without backscatter ($\gamma_{\mathrm{m}} = 0$). The corresponding Smagorinsky coefficient is $c_{\mathrm{S}} = [2/(3\alpha)]^{3/4}/\pi = 0.165$. The second case repeats this simulation but with backscatter. Two further cases are considered with enlarged or reduced diffusivities to see the sensitivity to the SGS model and to test Mason's (1994) hypothesis of arbitrary selection of filter scale relative to the grid scale, giving different Smagorinsky coefficients. These two cases ignore backscatter but use diffusivities which result from larger or smaller filter scales, 2Δ (i.e. larger diffusivities with $c_{\mathrm{S}} = 0.330$), and $\frac{1}{2}\Delta$ (smaller diffusivities, $c_{\mathrm{S}} = 0.083$).

Figure 3 shows the decay of the mean kinetic energy $E(t)$ of the flow versus time.

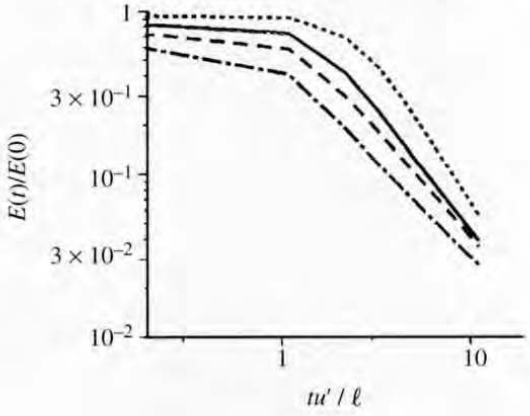

Figure 3. Normalized mean kinetic energy $E(t)/E(0)$ versus turn-over time tu'/ℓ. Full curve: without backscatter, long-dashed: with backscatter for standard eddy viscosity, short-dashed: without backscatter for reduced eddy viscosity, dash-dotted: without backscatter for increased eddy viscosity.

As expected, the differences between the cases with and without backscatter for the same filter scale are relatively minor. The good agreement in the decay rate between cases with and without random SGS motions shows that backscatter leaves the net dissipation rate essentially unaltered. However, as becomes more obvious from figure 4, the decay approaches power laws $E(t)/E(0) \sim t^{-n}$ with exponents n which do depend on backscatter. For the reference case without backscatter $n \cong 1.5$, whereas with backscatter $n \cong 1.33$. The asymptotic decay rate depends on the shape of the energy spectrum at small wavenumbers. The expected values are $n = 1.34$ from the experiments of Warhaft & Lumley (1978), 1.38 from the theory as given in Lesieur (1993, p. 195), and 1.37 from the numerical results of Métais & Lesieur (1992) (see also Chasnov 1994). An ideal agreement with these results should not be expected because of the limited integration period and the relatively small number of grid cells in our simulation. Tests have shown that n increases for smaller γ_m in agreement with the theory (Lesieur 1993, p. 195) which predicts that n grows and approaches $10/7 = 1.43$ for vanishing backscatter. A doubling or halving of the filter scale causes much different and unrealistic values 1.83 and 1.13. Obviously, the correct decay law can only be simulated with backscatter.

Figure 5 shows the resultant energy spectrum at the end of the simulation period. These normalized spectra change very little at times $tu'/\ell > 6$. Obviously, the spectrum is fairly close to what one expects in the inertial subrange. The LES with the nominal diffusivities both with and without backscatter give spectra which values are close to one in this normalization with $\alpha \cong 1.6$. This is an important fact and shows the consistency of the SGS model with the inertial range spectra. Backscatter causes a slightly wider inertial range with more energy at small wavenumbers, as expected. There is only a slight tendency for increasing energy near the cut-off wavenumber. From further simulations with different values of c_B (i.e. different diffusivities and backscatter rates) we found that the small-scale energy grows strongly when reducing c_B. On the other hand, the runs with doubled or halved filter scales show totally unrealistic spectra. They demonstrate that a reduced viscosity gives effects completely different from those of backscatter. Thus, we cannot support corresponding

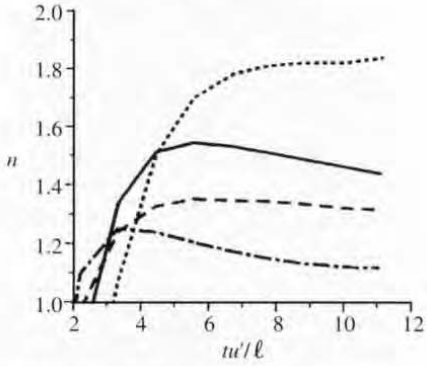

Figure 4. Exponent n in $E(t)/E(0) \sim t^{-n}$ versus turn-over time tu'/ℓ. Curves as in figure 3.

Figure 5. Normalized energy spectrum $E(k)/(\alpha\epsilon^{2/3}k^{-5/3})$ versus integer wavenumber $k/k_{\min}$ at $tu'/\ell = 11.1$. Curves as in figure 3.

suggestions (Germano *et al.* 1991; Andrén *et al.* 1994). Moreover, the results indicate that the filter scale is not a free parameter, but strictly related to the grid-scale. An increased filter scale implies stronger eddy diffusivities which causes more smoothing but nevertheless stronger dissipation because the smallest scales still contribute to the dissipation rate.

5. Conclusions

SGS stresses (and fluxes), other than the classical Reynolds stresses, contain random components in addition to parts which depend deterministically on the resolved fields. As a consequence of the random components, the stresses (fluxes) are only weakly correlated with the resolved strain rates (temperature gradients). The random stresses (fluxes) also induce random accelerations (temperature changes). Because of their finite Lagrangian timescales, these random sources transfer energy (variance) from SGS motions to resolved motion scales representing the backscatter of kinetic energy (variance). Without such history, unphysically large acceleration amplitudes are required to describe the same amount of backscatter. With backscatter, the eddy diffusivities are larger than without, as required to dissipate energy backscattered from the small scales. In spite of the reduction of backscatter by pressure forces, the backscatter process is more efficient for momentum than for heat transfer, causing increased turbulent Prandtl numbers, because of the fourth-order interactions of velocities as opposed to only second-order interactions between temperature and velocity fluctuations. However, spatial filtering in a numerical scheme reduces these effects more strongly for velocities than for temperature.

In order to model the effects of random SGS motions, a SGS model has been formulated which allows to represent backscatter in finite-difference versions of LES. The model provides realizable random Reynolds stresses and scalar fluxes because they are constructed as quadratic expressions of random fields. Thus they give a positive definite stress tensor and guarantee correlation coefficients between velocity and scalar fluctuations not exceeding unity in magnitude. The random stresses cause finite accelerations with the correct k^4 spectrum of backscatter forcing. The model accounts for the effect of incompressibility of both the SGS motions v_i and the forcing

r_i of resolved motions. These conditions were enforced by solving Poisson equations. The alternative of generating velocities v_i from a random vector potential cannot be recommended because it gives a too steep backscatter spectrum. For simplicity, we have assumed that the random SGS motions have a Gaussian probability density function. Distributions with flatness factors $F > 3$ are likely due to non-zero cumulants and intermittency, and would increase the backscatter for energy and reduce the correlation between stresses and strain rates, see equations (3.28) and (4.11). As long as SGS velocities and temperatures can be treated as independent random fields, the scalar fluxes are insensitive to such higher moments.

As expected, backscatter in the inertial subrange scales with the corresponding net dissipation rates. For $\gamma = 1$, and for EDQNM estimates of the timescales, the model predicts c_B in between 0.5 and 2.5 and c_{BT} in between 0.4 and 1.1, depending on the discrete representation of stresses and fluxes. For $\gamma \cong 0.7$, the values match the results of more complex spectral closure models (Leslie & Quarini 1979) and corresponding estimates by MT. Furthermore, the model quantifies the rather strong reduction of the correlation between stresses and strain rates by random motions. This reduction is consistent with previously computed or measured correlations. Unfortunately, no data exist to test the corresponding correlation for heat fluxes which we expect to be larger than for stresses.

For each kind of fluxes, the models contain essentially two open model parameters, the fractions γ of random stress components, and the timescale coefficients $c_{\tau v}$ and $c_{\tau\theta}$ of the random velocity and temperature fields. The timescales for stresses and heat fluxes are the inverse sums of these timescales. From EDQNM results, we find that the timescales are different for stresses and fluxes. Ideally, the coefficients γ should be determined such that the model gives the same ensemble mean variance of the random flux components as can be measured in real turbulent flows, see equation (3.14). The timescales should be measured according to equation (3.23). Such measurements are not yet available. Nevertheless, we expect that the values given in this paper provide proper estimates.

The model has been formulated as an extension of the Smagorinsky–Lilly model, but could also be introduced in other models which predict the SGS stresses as a deterministic function of the resolved fields. An interesting alternative is that of Bardina *et al.* (1980) combining the Smagorinsky model (possibly in a dynamical form as described in Germano *et al.* (1991), or in a split form as discussed by Sullivan *et al.* (1994)) with the stresses at the smallest resolved scales. This is attractive because of the high correlation between SGS stresses and the model stresses (see also Domaradzki *et al.* 1993). Backscatter may also be represented using transport equations for SGS stresses and fluxes, similar to those given by Launder *et al.* (1975), because such a model would predict SGS fluxes out of phase with the production terms. Perhaps, they also explain systematic counter-gradient SGS-stresses as observed by Härtel & Kleiser (1992). However, without random components such models would miss the stochastic nature of SGS motions.

The present model has been tested numerically. In the code, random fields are generated with proper Lagrangian timescales using a Langevin-type equation with the required Galilean invariance. The extended LES model describes stochastic effects of random SGS motions. However, the model extension essentially doubles the computing effort required for numerical integration. For decaying isotropic turbulence, the effect of backscatter is essential in predicting the proper power law of decay of energy with time. However, the effects of backscatter are small compared to the sensitivity

with respect to the effective filter scale. This confirms previous expectations that any SGS model which gives the correct amount of dissipation is sufficient when the grid resolves the inertial subrange. Therefore, stochastic backscatter models should be applied only in situations where a large fraction of energy and variance is carried by the SGS motions, and where grid refinement does not reduce this fraction considerably. This is typically the situation near walls. Otherwise, it would be better to spend the extra amount of computer time to increase the resolution of the LES. However, the concept of random stresses and stochastic backscatter may have implications for simulations which are necessarily coarsely resolving. This is the case, e.g. in numerical weather prediction models where predictability is an issue. It might be also relevant for global climate models where the resolved variability of the flow is often smaller than observed. For such applications the model parameters might be determined by using measured or computed high-resolution motion fields.

Appendix A. Backscatter in the non-local approximation of the EDQNM

The effects of backscatter can be estimated by using the spectral EDQNM model, as described by Lesieur (1993) and used in Chasnov (1991) and MT. The full EDQNM model includes non-local and near-local interactions in wavenumber space which we cannot evaluate analytically. Therefore, we restrict the following discussion to the non-local approximation (Lesieur 1993, pp. 193, 224) which describes the effects of SGS motions at wavenumbers greater than the cut-off wavenumber k_c with respect to the energy drain and backscatter from or into the large-scale motion field at $k \ll k_c$.

Depending on the spectra of kinetic energy $E(k)$ and of half the temperature variance $E_T(k)$, the SGS motions cause transfer of energy (variance) from small to large scales at rates $P(k)$ ($P_T(k)$) and backscatter from small to large scales at rates $B(k)$ ($B_T(k)$) per unit wavenumber. The non-local EDQNM approximations for these transfer spectra are

$$P(k) = 2K_\mathrm{m}k^2E(k), \quad P_T(k) = 2K_\mathrm{h}k^2E_T(k), \tag{A 1}$$

$$K_\mathrm{m} = \frac{1}{15}\int_{k_c}^{\infty} \vartheta_{0pp}\left[5E(p) + p\frac{\partial E(p)}{\partial p}\right]\mathrm{d}p, \quad K_\mathrm{h} = \frac{2}{3}\int_{k_c}^{\infty} \vartheta^T_{0pp}E(p)\,\mathrm{d}p, \tag{A 2}$$

$$B(k) = \tfrac{14}{15}k^4\int_{k_c}^{\infty} \vartheta_{0pp}\frac{E(p)^2}{p^2}\,\mathrm{d}p, \quad B_T(k) = \tfrac{4}{3}k^4\int_{k_c}^{\infty} \vartheta^T_{0pp}\frac{E(p)E_T(p)}{p^2}\,\mathrm{d}p, \tag{A 3}$$

with diffusivities K_m, K_h for momentum and heat, and triad relaxation times as a function of wavenumber p,

$$\vartheta_{0pp} = \frac{1}{2a_1}\left\{\int_0^p k^2E(k)\,\mathrm{d}k\right\}^{-1/2}, \quad \vartheta^T_{0pp} = \frac{1}{a_2+a_3}\left\{\int_0^p k^2E(k)\,\mathrm{d}k\right\}^{-1/2}. \tag{A 4}$$

These timescales contain the essential empiricism of EDQNM (see Herring *et al.* 1982), and are adjusted to match the expected inertial range spectra,

$$E(k) = \alpha\epsilon^{2/3}k^{-5/3}, \quad E_T(k) = \beta\epsilon_T\epsilon^{-1/3}k^{-5/3}, \tag{A 5}$$

as a function of corresponding mean dissipation rates ϵ and ϵ_T with Kolmogorov's and Batchelor's coefficients, which we take as $\alpha = 1.6$, $\beta = 0.67$.

When these spectra extend over all wavenumbers $k > 0$, the timescales are

$$\vartheta_{0pp} = [a_1 3^{1/2}\alpha^{1/2}\epsilon^{1/3}p^{2/3}]^{-1}, \quad \vartheta^T_{0pp} = [(a_2+a_3)3^{1/2}\alpha^{1/2}\epsilon^{1/3}p^{2/3}/2]^{-1}. \tag{A 6}$$

With these results equation (A 3) shows that contributions from SGS motions to backscatter decrease with p^{-6} for wavenumbers $p > k_c$ in the inertial subrange. Moreover, we obtain

$$K_m = \frac{\alpha^{1/2}\epsilon^{1/3}k_c^{-4/3}}{6a_1 3^{1/2}}, \quad K_h = \frac{\alpha^{1/2}\epsilon^{1/3}k_c^{-4/3}}{(a_2+a_3)3^{1/2}}, \tag{A 7}$$

$$B(k) = \frac{14\alpha^{3/2}}{75a_1 3^{1/2}}\frac{k^4}{k_c^5}\epsilon = 5c_B\frac{k^4}{k_c^5}\epsilon, \quad B_T(k) = \frac{8\alpha^{1/2}\beta}{15(a_2+a_3)3^{1/2}}\frac{k^4}{k_c^5}\epsilon_T = 5c_{BT}\frac{k^4}{k_c^5}\epsilon_T. \tag{A 8}$$

Here, the backscatter coefficients c_B and c_{BT} are introduced to match the integrals,

$$B \cong \int_0^{k_c} B(k)\,\mathrm{d}k = c_B\epsilon, \quad B_T \cong \int_0^{k_c} B_T(k)\,\mathrm{d}k = c_{BT}\epsilon_T. \tag{A 9}$$

They can be evaluated when a_1 and $a_2 + a_3$ were known. Herring *et al.* (1982) derive $a_1 = 0.36 = 0.22\alpha^{3/2}$ in agreement with Leslie & Quarini (1979) and Chasnov (1991). The ratio $(a_2+a_3)/a_1$ is estimated to be in between 2.0 and 3.61 according to Herring *et al.* (1982).

We stress that the integrals give only approximate results because the spectra are valid only for $k \ll k_c$. Nevertheless, for a self-contained estimate of the timescale coefficients a_1 and $a_2 + a_3$, we ignore this limitation and require local equilibrium such that

$$\epsilon = \int_0^{k_c} [P(k) - B(k)]\,\mathrm{d}k, \quad \epsilon_T = \int_0^{k_c} [P_T(k) - B_T(k)]\,\mathrm{d}k. \tag{A 10}$$

Similar assumptions were used by Lilly (1967) and others to evaluate SGS model coefficients but ignoring backscatter. With backscatter one obtains

$$a_1 = \frac{319\alpha^{3/2}}{3^{1/2}1500} = 0.123\alpha^{3/2}, \quad a_2 + a_3 = \frac{209\alpha^{1/2}\beta}{3^{1/2}150} = 2.74a_1, \tag{A 11}$$

$$\frac{\vartheta^T_{0pp}}{\vartheta_{0pp}} = \frac{2a_1}{a_2+a_3} = \frac{319\alpha}{1045\beta} = 0.73, \tag{A 12}$$

$$K_m = \frac{250}{319}\frac{1}{\alpha}\epsilon^{1/3}k_c^{-4/3} = 0.49\epsilon^{1/3}k_c^{-4/3}, \quad K_h = \frac{150}{209}\frac{1}{\beta}\epsilon^{1/3}k_c^{-4/3} = 1.07\epsilon^{1/3}k_c^{-4/3}, \tag{A 13}$$

$$c_B = \frac{56}{319} = 0.176, \quad c_{BT} = \frac{16}{209} = 0.077, \tag{A 14}$$

$$Pr_{SGS} = \frac{K_m}{K_h} = \frac{1045\beta}{957\alpha} = 0.46, \quad \frac{c_{BT}}{c_B} = \frac{638}{1463} = 0.44. \tag{A 15}$$

This approximate analysis identifies the dependence on the parameters α and β. However, the non-local model underestimates the stronger backscatter near the cut-off wavelength. Larger spectra $B(k)$ and $B_T(k)$ would cause greater values of the coefficients a_1 and $a_2 + a_3$. The present result for a_1 is 44% smaller than that given by Herring *et al.* (1982) while $(a_2 + a_3)/a_1$ is within the given range or values.

The ratio c_{BT}/c_B has been estimated by MT similarly for given turbulent Prandtl number. We don't know how this ratio would change if the near-local interactions get included in the EDQNM model. The turbulent Prandtl number Pr_{SGS} lies within the range of values used in LES (Schmidt & Schumann 1989). For $k_c = \pi/\Delta$, the above results give diffusivities in good agreement with equation (4.6),

$$K_m = \frac{250}{\pi 319\alpha}\left(\frac{2}{3\alpha}\right)^{1/2} e^{1/2}\Delta = 0.101 e^{1/2}\Delta, \quad K_h = K_m/Pr_{\mathrm{SGS}} = 0.220 e^{1/2}\Delta. \tag{A 16}$$

These diffusivities describe the total drain of energy from the large scales balancing in part the backscatter and are greater than required for net dissipation, therefore.

References

Andrén, A., Brown, A., Graf, J., Mason, P. J., Moeng, C.-H., Nieuwstadt, F. T. M. & Schumann, U. 1994 Large-eddy simulation of a neutrally stratified boundary layer: a comparison of four computer codes. *Q. J. R. Meteor. Soc.* **120**, 1457–1484.

Antonopoulos-Domis, M. 1981 Aspects of large eddy simulation of homogeneous isotropic turbulence. *Int. J. Numer. Meth. Fluids* **1**, 273–290.

Bardina, J., Ferziger, J. H. & Reynolds, W. C. 1980 Improved subgrid scale models for large eddy simulation. *AIAA* 80-1357, pp. 1–9.

Bertoglio, J. P. 1985 A stochastic-grid model for sheared turbulence. In *Macroscopic modelling of turbulent flows* (ed. U. Frisch, J. B. Keller, G. Papanicolaou & O. Pironneau), pp. 100–119. Springer.

Borgas, M. S. & Sawford, B. L. 1994 Stochastic equations with multifractal random increments for modelling turbulent dispersion. *Phys. Fluids* **6**, 618–633.

Chasnov, J. R. 1991 Simulation of the Kolmogorov inertial subrange using an improved subgrid model. *Phys. Fluids* A **3**, 188–200.

Chasnov, J. R. 1994 Similarity states of passive scalar transport in isotropic turbulence. *Phys. Fluids* **6**, 1036–1051.

Chen, H., Herring, J. R., Kerr, R. M. & Kraichnan, R. H. 1989 Non-Gaussian statistics in isotropic turbulence. *Phys. Fluids* A **1**, 1844–1854.

Clark, R. A., Ferziger, J. H. & Reynolds, W. C. 1979 Evaluation of subgrid-scale models using an accurately simulated turbulent flow. *J. Fluid Mech.* **91**, 1–16.

Deardorff, J. W. 1970 A numerical study of three-dimensional turbulent channel flow at large Reynolds number. *J. Fluid Mech.* **41**, 453–480.

Domaradzki, J. A., Wei Liu & Brachet, M. E. 1993 An analysis of subgrid-scale interactions in numerically simulated isotropic turbulence. *Phys. Fluids* A **5**, 1747–1759.

Domaradzki, J. A., Wei Liu, Härtel, C. & Kleiser, L. 1994 Energy transfer in numerically simulated wall-bounded turbulent flows. *Phys. Fluids* **6**, 1583–1599.

Fox, D. G. & Lilly, D. K. 1972 Numerical simulation of turbulent flows. *Rev. Geophys. Space Phys.* **10**, 51–72.

Gardiner, C. W. 1983 *Handbook of stochastic methods.* Springer.

Germano, M. 1992 Turbulence: the filtering approach. *J. Fluid Mech.* **238**, 325–336.

Germano, M., Piomelli, U., Moin, P. & Cabot, W. H. 1991 A dynamic subgrid-scale eddy viscosity model. *Phys. Fluids* A **3**, 1760–1765.

Gerz, T. & Palma, J. M. L. M. 1994 Sheared and stably stratified homogeneous turbulence: comparison of DNS and LES. In *Direct and large-eddy simulation* (ed. P. Voke, L. Kleiser & J. P. Chollet), pp. 145–156. Dordrecht, Netherlands: Kluwer.

Ghosal, S., Lund, T. S. & Moin, P. 1992 A dynamic localization model for large-eddy simulation of turbulent flows. Center for Turbulence Research, CTR Manuscript 139.

Härtel, C. & Kleiser, L. 1992 Comparative testing of subgrid-scale models for wall-bounded turbulent flows. In *Computational Fluid Dynamics '92* (ed. Ch. Hirsch *et al.*), vol. I, pp. 215–222. Amsterdam: Elsevier.

Herring, J. R., Schertzer, D., Lesieur, M., Newman, G. R., Chollet, J. P. & Larcheveque, M. 1982 A comparative assessment of spectral closures as applied to passive scalar diffusion. *J. Fluid Mech.* **124**, 411–437.

Horiuti, K. 1989 The role of the Bardina model in large eddy simulation of turbulent channel flows. *Phys. Fluids* A **1**, 426–428.

Kaltenbach, H.-J., Gerz, T. & Schumann, U. 1994 Large-eddy simulation of homogeneous turbulence and diffusion in stably stratified shear flow. *J. Fluid Mech.* **280**, 1–40.

Kraichnan, R. H. 1976 Eddy viscosity in two and three dimensions. *J. Atmos. Sci.* **33**, 1521–1536.

Launder, B. E., Reece, G. J. & Rodi, W. 1975 Progress in the development of a Reynolds-stress turbulence closure. *J. Fluid Mech.* **68**, 537–566.

Leith, C. E. 1990 Stochastic backscatter in a subgrid-scale model: plane shear mixing layer. *Phys. Fluids* A **2**, 297–299.

Leonard, A. 1974 Energy cascade in large-eddy simulations of turbulent fluid flows. *Adv. Geophys.* A **18**, 237–248.

Lesieur, M. 1993 *Turbulence in fluids*, 2nd revised edn. Dordrecht, Netherlands: Kluwer.

Leslie, D. C. & Quarini, G. L. 1979 The application of turbulence theory to the formulation of subgrid modelling procedures. *J. Fluid Mech.* **91**, 65–91.

Lilly, D. K. 1967 The representation of small-scale turbulence in numerical simulation experiments. In *Proc. IBM Sci. Comput. Symp. on Environmental Sci.* (ed. H. H. Goldstine), pp. 195–210. IBM Form no. 320-1951. Thomas J. Watson Research Center, Yorktown Heights, NY.

Lund, T. S. & Novikov E. A. 1992 Parameterization of subgrid-scale stress by the velocity gradient tensor. In *Annual Research Briefs – 1992*, pp. 27–43. Center for Turbulence Research, Stanford University.

Mason, P. J. 1994 Large-eddy simulation: a critical review. *Q. J. R. Meteor. Soc.* **120**, 1–26.

Mason, P. J. & Thomson, D. J. 1992 Stochastic backscatter in large-eddy simulations of boundary layers. *J. Fluid Mech.* **242**, 51–78.

Mason, P. J. & Brown, A. R. 1994 The sensitivity of large-eddy simulations of turbulent shear flow to subgrid models. *Bound.-Layer Meteor.* **70**, 133–150.

Meneveau, C. 1994 Statistics of turbulence subgrid-scale stresses: necessary conditions and experimental tests. *Phys. Fluids* **6**, 815–833.

Métais, O. & Lesieur, M. 1992 Spectral large-eddy simulation of isotropic and stably stratified turbulence. *J. Fluid Mech.* **239**, 157–194.

Nieuwstadt, F. T. M., Mason, P. J., Moeng, C.-H. & Schumann, U. 1993 Large-eddy simulation of the convective boundary layer: a comparison of four computer codes. In *Turbulent Shear Flows 8* (ed. F. Durst, R. Friedrich, B. E. Launder, F. W. Schmidt, U. Schumann & J. H. Whitelaw), pp. 343–367. Springer.

Orszag, S. A. 1970 Analytical theories of turbulence. *J. Fluid Mech.* **41**, 363–386.

Piomelli, U., Cabot, W. H., Moin, P. & Lee, S. 1991 Subgrid-scale backscatter in turbulent and transitional flows. *Phys. Fluids* A **3**, 1766–1771.

Reynolds, O. 1895 On the dynamical theory of incompressible viscous fluids and the determination of the criterion. *Phil. Trans. R. Soc. Lond.* **186**, 123–164.

Reynolds, W. C. 1990 The potential and limitations of direct and large-eddy simulations. In *Whither turbulence?* (ed. J. L. Lumley), pp. 313–343. Springer.

Rose, H. A. 1977 Eddy diffusivity, eddy noise and subgrid-scale modelling. *J. Fluid Mech.* **81**, 719–734.

Schmidt, H. & Schumann, U. 1989 Coherent structure of the convective boundary layer deduced from large-eddy simulation. *J. Fluid Mech.* **200**, 511–562.

Schumann, U. 1975 Subgrid scale model for finite difference simulations of turbulent flows in plane channels and annuli. *J. Comput. Phys.* **18**, 376–404.

Schumann, U. 1977 Realizability of Reynolds-stress turbulence models. *Phys. Fluids* **20**, 721–725.

Schumann, U. & Patterson Jr, G. S. 1978 Numerical study of pressure and velocity fluctuations in nearly isotropic turbulence. *J. Fluid Mech.* **88**, 685–709.

Schumann, U. & Sweet, R. A. 1988 Fast Fourier transforms for direct solution of Poisson's equation with staggered boundary conditions. *J. Comput. Phys.* **75**, 123–137

Smagorinsky, J. 1963 General circulation experiments with the primitive equations. I. The basic experiment. *Mon. Weather Rev.* **91**, 99–164.

Sullivan, P. P., McWilliams, J. C. & Moeng, C.-H. 1994 A subgrid-scale model for large-eddy simulation of planetary boundary-layer flows. *Bound.-Layer Meteor.* **71**, 247–276.

Warhaft, Z. & Lumley, J. L. 1978 An experimental study of decay of temperature fluctuations in grid generated turbulence. *J. Fluid Mech.* **88**, 659–684.